Chapter 9
Electrodes Based on Carbon Nanomaterials: Structure, Properties, and Application to Capacitive Deionization in Static Cells

Yurii Volfkovich, Daniil Bograchev, Alexey Mikhalin, Alexey Rychagov, Valentin Sosenkin, Vitaly Milyutin, and Daewook Park

9.1 Capacitive Deionization

Deionization processes, which are driven by electrical field, can be divided to two types. The first type is electrodeionization (EDI) that involves ion exchange and transport of charged species through the ion-exchanger bed and membranes [1, 2]. This method allows one to remove from water not only ions of alkaline metals, sulfate, and halogenides [1–3] but also transition metal cations [4, 5]. The second type is capacitive deionization (CDI); it is a promising and the most cost-effective method of water desalination [5–14]. An electric field affects adsorption of anions and cations on positive and negative electrodes, respectively, under low applied voltage (it is not sufficiently higher than 1.2 V). Highly dispersive carbon electrodes (HDCE) with a specific surface area of 500–3000 $m^2\ g^{-1}$ are used in CDI processes. The electric double layer (EDL) is charged similarly to that in electrochemical supercapacitors (ESCs), which results in deionization of the solution. Under polarity reversal or short circuit of the electrodes, ions diffuse from the interface back to the solution. This provides energy regeneration and concentrating of the solution that is removed from the cell. The deionization stage corresponds to the charging of the supercapacitor, while the concentrating stage (regeneration) is related to its discharging.

As compared with other methods of water desalination, sufficient advantages of CDI are as follows: low cost (about one third of the value of the closest competing process, reverse osmosis), high cycleability of the electrodes, and low maintenance costs. Moreover, chemical stability of the electrodes excludes permeation of foreign

Y. Volfkovich · D. Bograchev (✉) · A. Mikhalin · A. Rychagov · V. Sosenkin · V. Milyutin
A. N. Frumkin Institute of Physical Chemistry and Electrochemistry of the Russian Academy of Sciences, Moscow, Russia

D. Park
Samsung Electronics Co., Ltd, Gyeonggi-do, South Korea

O. Fesenko, L. Yatsenko (eds.), *Nanooptics, Nanophotonics, Nanostructures, and Their Applications*, Springer Proceedings in Physics 210,
https://doi.org/10.1007/978-3-319-91083-3_9

substances in the purified water. CDI is effective for treatment of water of different salinity: this method allows reducing the ion concentration down to a very low level. Finally, practically no insoluble compounds are precipitated inside the electrode pores. CDI is applied in desalination of brackish and sea water, as well as for softening of tap water, particularly for deionization of water supplied into washing machines.

Electrode materials for CDI are developed from the past years. Different types of both single-component (activated carbon, aerogels, nanotubes, graphene, etc.) [14–17] and carbon-based composite materials (carbon-carbon composite, carbon-metal oxide composite, carbon-polymer composite, and carbon-polymer-metal oxide composite) [18–21] have been suggested. Mesoporous materials (i.e., containing nanosized pores) are considered as main suitable electrodes for CDI, since these pores make significant contribution to surface area. Moreover, ion transport in these pores is faster than that in micropores. As known, porous structure of carbon materials includes both hydrophilic and hydrophobic pores [22–24]. Electrical double layer (EDL) that is responsible for adsorption capacitance of carbon exists only in hydrophilic pores. The aim of the investigation is to establish the effect of different types of nanopores on charge capacitance of carbon electrodes. This parameter determines the efficiency of CDI processes.

A number of models have been proposed for description of the CDI processes. Classical works [25–29] are used as a basis for the modeling of processes in porous CDI electrodes. In the absence of the electrolyte flux, CDI equations are similar to those in supercapacitor models [29], which are based on the theory of porous electrodes [30]. The first models of porous electrodes were proposed by de Levie more than 50 years ago [28, 29], but analytical models for discharge curves of supercapacitors have been obtained later [30]. Equation systems that describe the charging of the supercapacitor have been solved numerically [31].

More modern approaches consider electrosorption (EDL in a single pore) [32, 33], electrolyte transport along the electrodes and separator, as well as the charging of EDL of the electrodes [34–36] and surface conductivity (SC, tangential conductivity of EDL) [37–40]. Known CDI models require calculation of EDL inside pores of the electrodes. It is a very difficult problem, since it is necessary to consider the hydrophilicity-hydrophobicity of the electrodes, tortuosity, widenings-narrowings, intersections of pores, etc. The task of the investigation involves also modeling of CDI processes only based on parameters, which can be determined experimentally.

9.2 Carbon Electrodes and Their Characterization

Activated carbon textiles, such as CH900 (Curaray Co, Japan) and VISKUMAK (Neorganica LTD, RF), were used in the studies. SAIT-type electrodes (SAIT Co, South Korea) were also used. These materials were manufactured by compacting activated carbon powder together with a binder (polytetrafluorethylene, PTFE).

The method of standard contact porosimetry (MSCP) was used to study the electrode materials similarly to [41–44]. The MSCP allows one to investigate pore structure in a very wide interval of pore radius: from 1 nm to 100 μm. This technique can be applied to all materials. Besides carbon materials, pore size distributions were obtained for gas diffusion layers of electrodes for fuel cells [22, 41, 42, 45], dispersed platinum [46], polymer membranes [47], ion exchange resins [3, 5, 48], peat [42, 44], paper [42], and many other objects.

Before the measurements using water or octane, both the tested sample and standards were dried under vacuum at 170 °C.

Morphology of the electrodes was observed by means of a JSM-U3 scanning electron microscope (JEOL, Japan).

Adsorption capacity was determined as follows. A weighed sample of air-dried material (0.065 g) was inserted into the 0.2-M NaOH solution (20 cm^3); the liquid was stirred for 24 h. Then the effluent was titrated with an HCl solution using xylenol orange as an indicator. Adsorption capacity was calculated as $\frac{(c_0-c_e)V}{M}$ (here c_0 and c_e are the concentrations of the alkaline solution before and the treated solution, respectively; V is its volume, m is the sample mass).

Adsorption capacity with respect to Cu^{2+} ions (in fact, toward $[Cu(NH_3)_4]^{2+}$) was also determined. The 0.2 M solution of copper ammoniate (pH = 9.6) was used; the effluent was analyzed by titration with EDTA using murexide [49].

9.3 Study of CDI Process in Static Cell

In general, the electric capacitance of electrodes made of activated carbon is a sum of EDL capacitance and pseudocapacitance of Faraday reactions [27]. Hence, electric capacitance was measured and EDL capacitance was calculated on the basis of this value and used further for modeling of the CDI processes.

Galvanostatic measurements of dependences of cell voltage on time were carried out under the charging-discharging conditions in order to determine the EDL capacitance. A static cell was used, in which the electrolyte was only in the pores of the electrodes and separator. The cell design (Fig. 9.1) and methods of measurements were described in [31]. This type of cell simulates both single-cell and multicell electrochemical capacitors for bipolar assemblies with serially connected individual cells. The cell contained two electrodes of the same type with similar surface areas (2.5–3 cm^2). Graphite current collectors provided good contact with the electrodes and allowed working in strongly acidic and strongly basic media. The range of applied potentials was 0–1.5 V. The current distribution layer (foil) was located between the electrode and current collectors. The collector was manufactured by compressing the thermoexfoliated graphite powder with the further impregnation by molten paraffin.

The assembly also included a separator (Gore Co.) between two electrodes. The separator film was used as a capillary for the reference electrode. This cell design

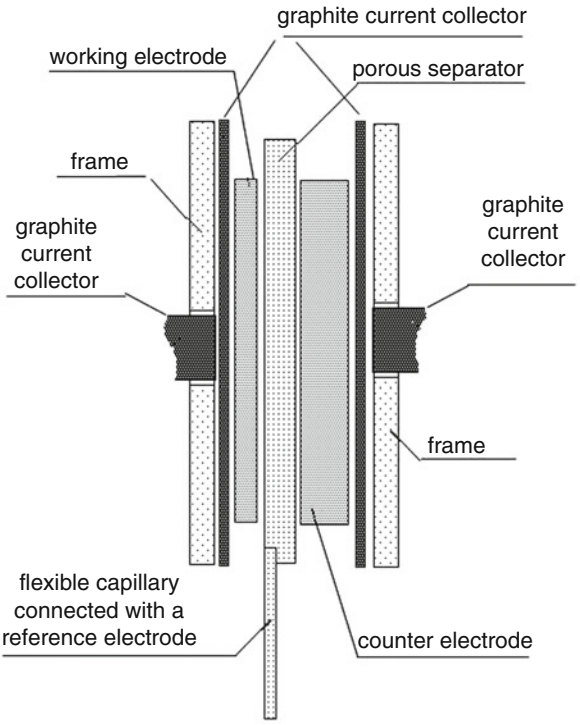

Fig. 9.1 Static electrochemical cell: scheme of electrode-separator assembly

allowed performing measurements according to both two- and three-electrode schemes. The electrodes were prewashed in a stream of deionized water and dried at 170° C under vacuum. Since the volume of electrolyte in electrode pores was extremely low (0.2–0.5 cm^3), oxygen was removed by conditioning the electrode for 10–15 min at the potential, which is close to that of hydrogen evolution. Electrochemical studies were carried out using a VoltaLab 40 potentiostat (Radiometer Analytical, France).

Galvanostatic measurements were performed in a static cell equipped by carbon electrodes. A change in the voltage during charging-discharging was controlled. Single-component $NaHCO_3$, $CaCl_2$, and $MgSO_4$ solutions of different concentrations (0.1, 0.5 and 1 g-eq dm^{-3}), as well as a mixed solution, were used as electrolytes. The composition of the mixed solution was as follows (mg-eq dm^{-3}): $NaHCO_3$ (4.4), $CaCl_2$ (11.9), $MgSO_4$ (10.7). This composition corresponded to brackish water. The capacitance values (C_c) were determined as:

$$C_{c,full} = \frac{2I_{full}\Delta t}{\Delta U} \tag{9.1}$$

where U is the cell voltage, I_{full} is current, t is the time.

Since adsorption capacity of the electrodes is proportional to capacitance of the electrode EDL ($C_{EDL,\ full}$), the change in the solution concentration (Δc) is:

$$\Delta c = \frac{C_{EDL,full}\Delta U}{2FV}, \tag{9.2}$$

where F is the Faraday constant and V is the solution volume. It was assumed in Eq. (9.2) that the adsorption efficiency of EDl charging is 100%. Expression (9.2) is also valid for electrodes of equal capacitance.

9.4 Porous Structure of Carbon Electrodes. Recognition of Micropores and Nanosized Voids

The principal MSCP data are given in Table 9.1; pore size distributions (obtained using both water and octane) are plotted vs effective pore radius (r^*) (Fig. 9.2). The r^* parameter is determined as [41, 42]:

$$r^* = \frac{r}{\cos\theta} \tag{9.3}$$

where r is the true value of pore radius and θ is the wetting angle for water. According to Eq. (9.3), the $\theta - \log r$ curves were plotted (Fig. 9.3). Since octane wets all materials almost perfectly, $r^* \approx r$ for this liquid.

The difference between the maximal content of octane and water (maximal values of curves I and II) corresponds to hydrophobic pores. The carbon electrodes were found to include both hydrophilic and hydrophobic pores (hydrophilic and hydrophobic specific surface area). The contact angle distributions show hydrophobicity for all electrodes, especially for the SAIT material containing particles of the hydrophobic PTFE binder (see Fig. 9.3). Complex $\theta - \log r$ dependences are due to inhomogeneous distribution of surface groups in pores of different size.

As follows from Fig. 9.2, the electrodes are characterized by a wide range of pore sizes: from r<1 nm to 100 μm. The porous structure of the electrodes includes both hydrophilic and hydrophobic porosity. High values of specific surface area differ noticeably (see Table 9.1). The values of hydrophilic and hydrophobic porosity are also different. The MSCP data for octane allow drawing some principal conclusions.

Table 9.1 Characteristics of porous structure of carbon electrodes

Electrode	Specific surface area, $m^2\ g^{-1}$		Ratio of hydrophilic and total surface areas	Porosity, $cm^3\ cm^{-3}$		
	Total	Hydrophilic		Total	Hydrophilic	Hydrophobic
CH900	1520	850	0.56	0.850	0.786	0.064
VISKUMAK	600	416	0.70	0.729	0.623	0.106
SAIT	940	520	0.55	0.715	0.490	0.225

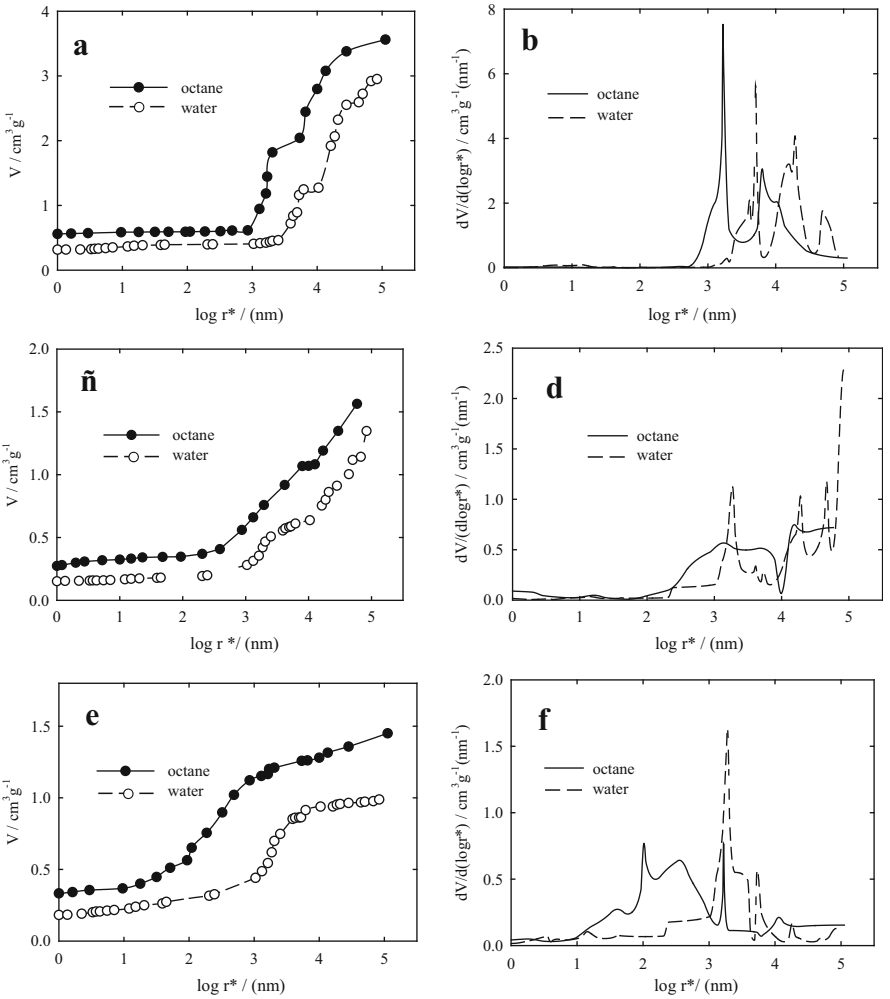

Fig. 9.2 Integral (**a**, **c**, **e**) and differential (**b**, **d**, **f**) pore size distributions for the CH900 (a, b), VISKUMAK (**c**, **d**), and SAIT (**e**, **f**) materials. The curves are plotted vs effective pore radius

Micropores, as well as large macropores, are characteristic for all materials. The volume of hydrophilic pores, which can be related to nanoobjects (r<50 nm) increases on the order: CH900 < VISKUMAK < SAIT. The total porosity (0.715–0.850) is sufficient for all electrodes.

Comparison of the data obtained in water and octane media shows higher hydrophilic porosity. The values of the total specific surface area of 600–1520 $m^2\ g^{-1}$ hydrophilic pores make sufficient contribution to it. This is very important, since EDL that determines the principal characteristics of the CDI processes exists on the

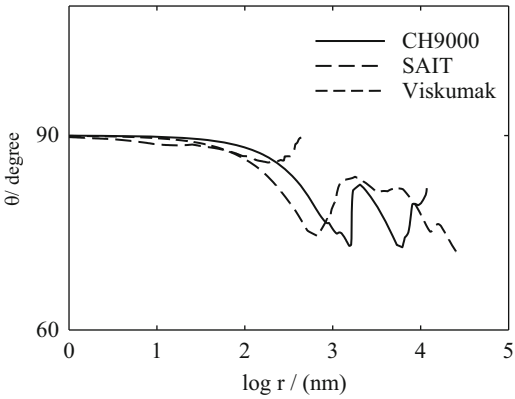

Fig. 9.3 Wetting angle distributions for the samples of carbon electrodes. The distributions were plotted vs true pore radius

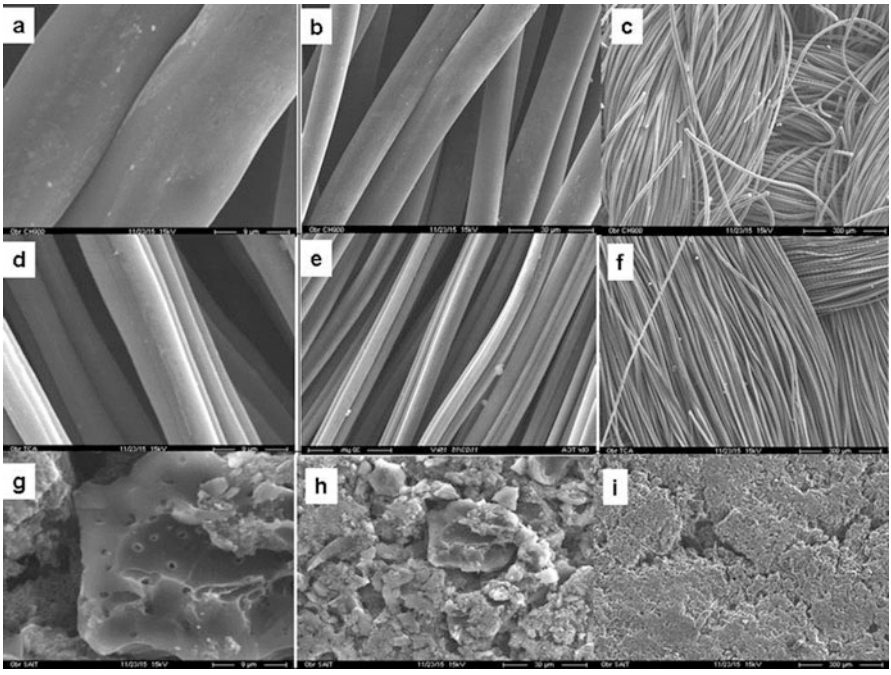

Fig. 9.4 SEM images of CH900 (**a**–**c**), VISKUMAK (**d**–**f**) textiles, and SAIT composite (**g**–**i**)

hydrophilic surface. The largest contribution of hydrophilic area into the total surface area has been observed for the VISKUMAK sample. Regarding the CH900 carbon material and SAIT composite, the ratios of hydrophilic and total surface areas are sufficiently lower and close to each other.

9.5 Morphology of Electrodes

Morphology of single-component materials and bicomponent SAIT composite are sufficiently different (Fig. 9.4). Large fibers of the CH900 sample are more disordered than those of the VISKUMAK, in which the fibers form ordered bundles. Voids between them correspond to the largest pores (see Fig. 9.2). Since the diameter of CH900 fibers is larger, the size of the corresponding pores is also larger as compared to the pores in the VISKUMAK sample. The specific surface area of the CH900 electrode is higher, indicating a more significant volume of micropores and small mesopores (r<5 nm) inside the fibers of this material.

The structure of the bicomponent SAIT sample is corpuscular-like. The material consists of particle agglomerates, the size of which is up to several tens of microns. These particles are evidently related to carbon bound to the polymer binder. Large massive particles (polymer binder) are also visible. Pores with the size of several microns to several tens of microns (see Fig. 9.4) correspond to spaces between agglomerates as well as to voids between them and the binder. Nanopores are mainly voids inside the particles.

9.6 Adsorption Capacity

Values of adsorption capacity are given in Table 9.2. The CH900 and VISKUMAK samples demonstrate the highest capacity with respect to Na^+. It should be noted that these values are higher in the case of fibrous single-component samples than those of Nafion-type membranes (0.8 0.9 mg-eq g^{-1} [50]). Despite a considerable difference in the hydrophilic specific surface area (see Table 9.1), the capacity values of the fibrous samples are close to each other. This means partial inaccessibility of the surface of the CH900 sample for Na^+ ions.

The difference between the values of adsorption capacity with respect to $[Cu(NH_3)_4]^{2+}$ is insignificant for all samples. Assuming ion exchange being the only mechanism, the experimental values were found to be higher than expected. The ratios of the experimental data and the calculated values are 1.3–1.4 (ACF) and 3.4 (SAIT). Thus, the larger content of surface groups that are responsible for specific adsorption of $[Cu(NH_3)_4]^{2+}$ species is characteristic for the SAIT sample. The capacity values are comparable with those for such inorganic ion exchangers as amorphous zirconium phosphate [51]. Since the structure as well as hydrophilic-

Table 9.2 Adsorption capacity of electrode materials

	Sorption capacity/mg-eq g^{-1}		
	Experimental values		Theoretical values
Material	Na^+	$[Cu(NH_3)_4]^{2+}$	
CH900	1.14	0.75	0.57
VISKUMAK	1.02	0.71	0.51
SAIT	0.37	0.62	0.18

hydrophobic and adsorption properties of the investigated materials is rather complex, it is difficult to predict their electrochemical behavior. Nevertheless, as shown in [52], adsorption capacity is proportional SC of the carbon electrodes. In its turn, SC affects conductivity of CDI cells. The maximal values of EDL capacitance are expected for the CH900 electrode due to the highest hydrophilicity and adsorption capacity.

9.7 Processes in Static Electrochemical Cell

In order to use the CDI model, it was necessary to obtain the values of specific EDL capacitance for each of the carbon electrodes and solutions of different salts of different concentrations. However, the current stage of development of electrochemistry offers no possibility for theoretical solution of this problem for microporous-mesoporous carbon electrodes. Owing to this, we have developed an experimental method to solve this task. The method involves measurements of electrochemical capacitance depending on the current. The capacitance values were determined on the basis of the measured galvanostatic curves using Eq. (9.1).

As an example, a dependence of integral capacitance of the CH900 electrode on current density is plotted in the insertion to Fig. 9.5. Decrease in current density results in growth of capacitance followed by a plateau and a rapid increase.

The increase in capacitance at 300–200 mA g^{-1} is caused by considerable ohmic losses under high current, as follows from insertion of Fig. 9.5. The decrease in current is accompanied by a decrease in ohmic losses. They become extremely low at 200–150 mA g^{-1} (plateau region) – the capacitance is determined only by the EDL. In the low current range, the contribution of pseudocapacitance of faradaic processes becomes significant. With respect to carbon electrodes, these processes are quasi-reversible redox reactions of their surface groups [27].

In the first approximation, specific capacitance of the EDL per mass unit (C_{EDL}) was estimated from the $C_{EDL,\ full}$value (see formula (9.2)), which is evaluated from the plateau data. For instance, C_{EDL}=63 (CH900, multicomponent solution) and 107 F g^{-1} (VISKUMAK, 1 N $CaCl_2$), as shown in Fig. 9.6.

The values of EDL capacitance per area unit (C^s_{EDL}) were also obtained. In this case, the C_{EDL} value was divided by the hydrophilic surface area from Table 9.1. The C_{EDL} and C^s_{EDL} values grow at an increase of the solution concentration. This is probably due the decreasing thickness of the diffuse part of EDL under these conditions. As a result, EDL can exist only in smaller pores. The values of EDL capacitance per unit of hydrophilic surface area are 9.2–26 μF cm^{-2}. With respect to CH900 and VISKUMAK textiles, the highest capacitance has been found for the 1:1 electrolyte ($NaHCO_3$), and the smallest values have been observed for the 2:2 electrolyte ($MgSO_4$). The data for the 1:2 electrolyte ($CaCl_2$) are in-between. It is possible to state the highest C_{EDL} value for the CH900 material that is characterized by the largest hydrophilic surface area (see Table 9.1) and the highest adsorption

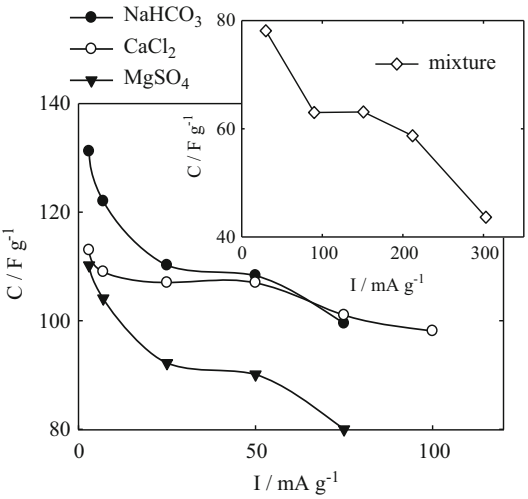

Fig. 9.5 Capacitance of the VISKUMAK electrode as a function of current density. One-component 1 N solutions were used. Masses (g) of the electrode and electrolyte were 0.076 and 0.28 ($NaHCO_3$), 0.033 and 0.19 ($CaCl_2$), and 0.058 and 0.21 ($MgSO_4$). The external electrode area was 3 ($NaHCO_3$) and 2.5 ($CaCl_2$, $MgSO_4$) cm^2. The same dependence for the CH900 electrode is plotted in the insertion. The curve was obtained for the multicomponent solution; masses of the electrode and electrolyte were 0.033 and 0.13 g, respectively

capacity (see Table 9.2). These characteristics are smallest for the SAIT composite that demonstrates the lowest values of EDL capacitance. Intermediate C_{EDL} values have been found for the VISKUMAK electrode. The highest C^s_{EDL} values have been obtained for this material. This is due to a large fraction of hydrophilic surface area that provides good connection between hydrophilic (electrochemically active) areas on the surface.

9.8 Modeling of Processes in Static Cell Involving Parameters Attributed to Hydrophilic Micropores and Nanosized Voids

Since the porous structure of AC involves a wide range of hydrophilic and hydrophobic pores (from <1 nm to 100 μm), exact calculation of C_{EDL} is practically impossible. Contrary to the known works, which involve models of electrosorption [32, 33], Donnan equilibrium [53, 54], and other approach (see above), an alternative point of view is developed. The model uses experimental SC [52] data as well as C_{EDL} values are obtained with account for hydrophilic and hydrophobic porosity of the electrodes. This approach allows one neglecting the thickness and composition of intraporous EDLs, their overlapping in weakly concentrated solutions, and absence in hydrophobic pores.

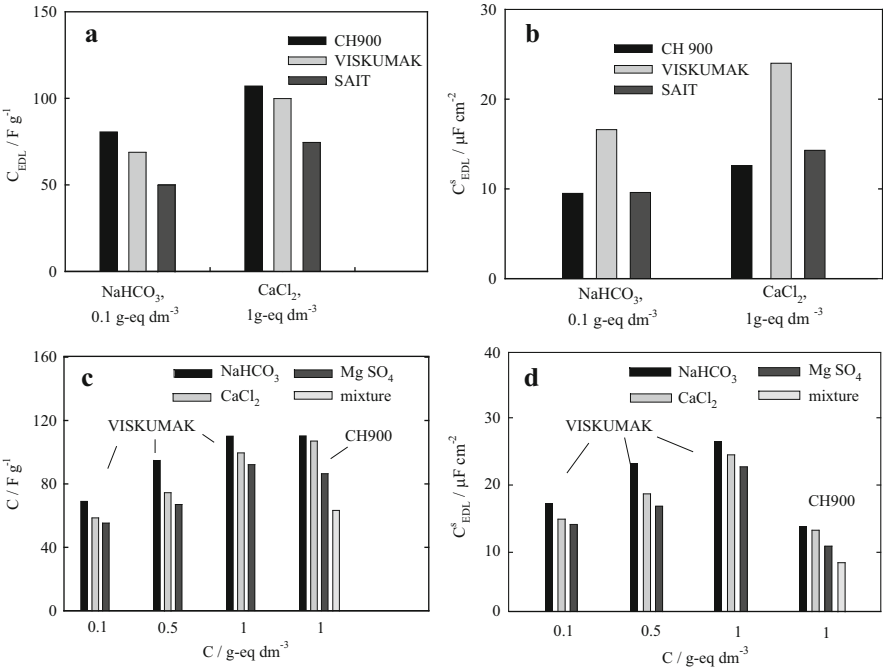

Fig. 9.6 Capacitance of EDL per mass unit (**a**, **c**) and per unit of hydrophilic surface area (**b**, **d**) for different carbon electrodes and different concentrations of electrolyte solutions

The following processes were considered: (i) charging-discharge of EDL, (ii) diffusion and migration of species, (iii) SC (the data [52] were used), (iv) specific adsorption of ions, and (v) characteristics of hydrophilic and hydrophobic pores. Both the EDL capacitance and SC are attributed to nanosized pores, which make sufficient contribution to the total specific surface area.

Application of supercapacitors to desalination of aqueous solutions is based on the properties of EDL of ideally polarized carbon electrodes. The charging of EDL causes adsorption of ions on the surface of the cathode and anode. i.e., removal of species from the solution. The main difference between an electrochemical cell for CDI and supercapacitor is usage of a diluted solution. The charging-discharging processes of EDL are characterized by reversibility and huge cycleability. Figure 9.7 illustrates the model with a simple 1D structure involving two porous carbon electrodes and a porous separator between them.

Resistance of carbon electrode is assumed to be neglected, since its conductivity is much higher than that of electrolyte. This assumption is justified due to the small concentration of hardness ions. For instance, the conductivity of the carbon electrode is about 10^5 S cm^{-1} (the conductivity of natural water containing hardness ions is about 2–3 mS cm^{-1}). Both the effective conductivity (κ) and effective diffusion coefficients D (through the electrode and separator) have to be corrected taking into consideration porous structure of the materials. The Archie's law is used [53–56]

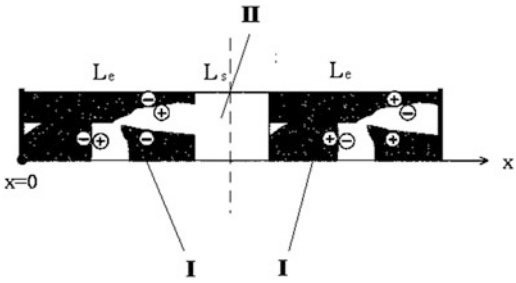

Fig. 9.7 Scheme of the cell model: (**I**) electrodes and (**II**) separator (spacer). The dashed line corresponds to the axis of symmetry of the problem. L_e is the thickness of the porous electrode. L_s is the thickness of the porous separator

$$\kappa = \kappa_1(c)\varepsilon^m; \;\; D = D_0\varepsilon^m, \tag{9.4}$$

where ε is the hydrophilic porosity, and D_0 is the diffusion coefficient of free electrolyte, m is the Archie's exponent that characterizes the influence of the porous structure on transport properties of electrolyte. $\kappa_1(c)$is bulk conductivity of free electrolyte that is a linear function of concentrations.

The mass transport in our model is described within a framework of the theory for a binary dilute solution [26, 34]:

$$\varepsilon\frac{\partial c}{\partial t} = D\frac{\partial^2 c}{\partial x^2} + \frac{C_s}{z_+F}A_s\frac{\partial \varphi}{\partial t}, \tag{9.5}$$

where φ is the electrical potential of electrolyte; C_s is the specific capacitance of electrode, which becomes zero for the separator; and A_s is the adsorption coefficient ($A_s = \left(t_+\frac{dq_+}{dq} - t_-\frac{dq_-}{dq}\right) \approx \pm\frac{1}{2}$ [34]). The charge transport in the electrolyte is described by the equation:

$$C_s\frac{\partial \varphi}{\partial t} = \frac{\partial}{\partial x}\left(\kappa_{eff}\frac{\partial \varphi}{\partial x}\right) + \frac{\partial}{\partial x}\left(\frac{\kappa_{eff}RT(t_+ - t_-)}{F}\frac{\partial \ln c}{\partial x}\right) \tag{9.6}$$

where t_+ and t_- are the transport numbers of cation and anion, respectively, and κ_{eff} is the effective conductivity. The latter term is a sum of conductivity with account for porosity and SC (κ_s) [52]. In other words, $\kappa_{eff} = \varepsilon^m\kappa_0\frac{c}{c_0} + \kappa_s$, where c_0 is the initial concentration, κ_0 is the electrolyte conductivity at the initial concentration. The method for SC measurements was described earlier [52]. The SC value is assumed to be proportional to the amount of adsorbed ions. This value is expressed as $C\sigma\frac{I_{full}t}{FV}$, where σ is the SC coefficient, which is the coefficient of proportionality between SC and adsorption capacity.

The problem is solved for a half-cell (the porous electrode and a half of the separator). The symmetry of the system with respect to boundary conditions is considered. On the left side ($x = 0$), the boundary conditions are:

$$\left.\frac{\partial c}{\partial x}\right|_{x=0} = 0; \quad \left.\frac{\partial \varphi}{\partial x}\right|_{x=0} = 0. \tag{9.7}$$

In the center of separator ($x = L_e + \frac{1}{2}L_s$):

$$\left.\frac{\partial c}{\partial x}\right|_{x=L_e+\frac{1}{2}L_s} = 0; \quad \kappa \left.\frac{\partial \varphi}{\partial x}\right|_{x=L_e+\frac{1}{2}L_s} = \frac{-I_{full}}{S}. \tag{9.8}$$

The initial conditions are:

$$c = c_0; \quad \varphi = 0 \tag{9.9}$$

As pointed out, the initial conditions must be corrected using specific adsorption. It is assumed that only specific adsorption of species occurs before charging. This results in a decrease in the initial concentration. Furthermore, the initial concentration was also a fitting parameter; its value was found by comparing the theoretical and experimental data, as shown further.

A pdepe function of the MATLAB program package that is based on the method of lines (MOL) [57] was used to solve the system of parabolic equations. The pdepe function allows solving the initial-boundary value problems for systems of parabolic and elliptic partial differential equations in the system with a single spatial variable and the time variable.

9.9 Comparison of Theoretical and Experimental Data for Static Cell

The solution of the system (9.4)–(9.6) with boundary conditions (9.7)–(9.8) and initial condition (9.9) can be obtained using numerical methods (Tables 9.3, and 9.4). Only hydrophilic porosity (see Table 9.1) was taken into consideration. Moreover, the values of EDL capacitance per unit of hydrophilic surface area were used. The separator parameters were as follows: the thickness was 1.5×10^{-5} m, porosity was 0.46, and the Archie's exponent was 2. For example, Fig. 9.8 shows the numerical solution for the voltage and mean $NaHCO_3$ concentration in the static cell, as well as evolution of the profile concentration in the half-cell in time.

Figure 9.9 illustrates theoretical and experimental galvanostatic curves of electrode charging. The C^s_{EDL} values obtained as described in Sect. 3.4 were used for calculations. The plots are $U-t$ dependences for different currents and solutions. The

Table 9.3 Properties of 0.1 N electrolytes

Salt	$D\times10^9$, $m^2\ s^{-1}$	κ, $Ohm^{-1}\ m^{-1}$	t_+
$NaHCO_3$	1.26×10^{-9}	1.014	0.53
$CaCl_2$	1.34×10^{-9}	0.882	0.41
$MgSO_4$	8.54×10^{-9}	0.497	0.37

Table 9.4 Model parameters (current density was 28 or 100 A m^{-2})

		Measured values			Fitted values	
Electrode	Electrolyte	Electrode thickness $\times 10^4$, m	Electrode porosity	Surface capacitance $\times 10^{-5}$, F m^{-2}	Archie's exponent	SC coefficient, S m^2 mol^{-1}
CH-900	$NaHCO_3$	4.67	0.63	2.6 or 2.1	2.0	0.2
CH-900	$CaCl_2$	4.67	0.63	2.4 or 2.6	2.0	0.2
CH-900	$MgSO_4$	4.67	0.63	2.2 or 2.4	2.0	0.2
VISKUMAK	$NaHCO_3$	6.04	0.69	2.6	2.0	0.1
VISKUMAK	$CaCl_2$	6.04	0.69	2.6	2.0	0.1
VISKUMAK	$MgSO_4$	6.04	0.69	2.6 or 2.8	2.0	0.2 or 0.1
SAIT	$NaHCO_3$	4.30	0.47	2.4	2.8	0.2
SAIT	$CaCl_2$	4.30	0.47	2.6	2.0	0.1
SAIT	$MgSO_4$	4.30	0.47	2.4	2.8	0.2

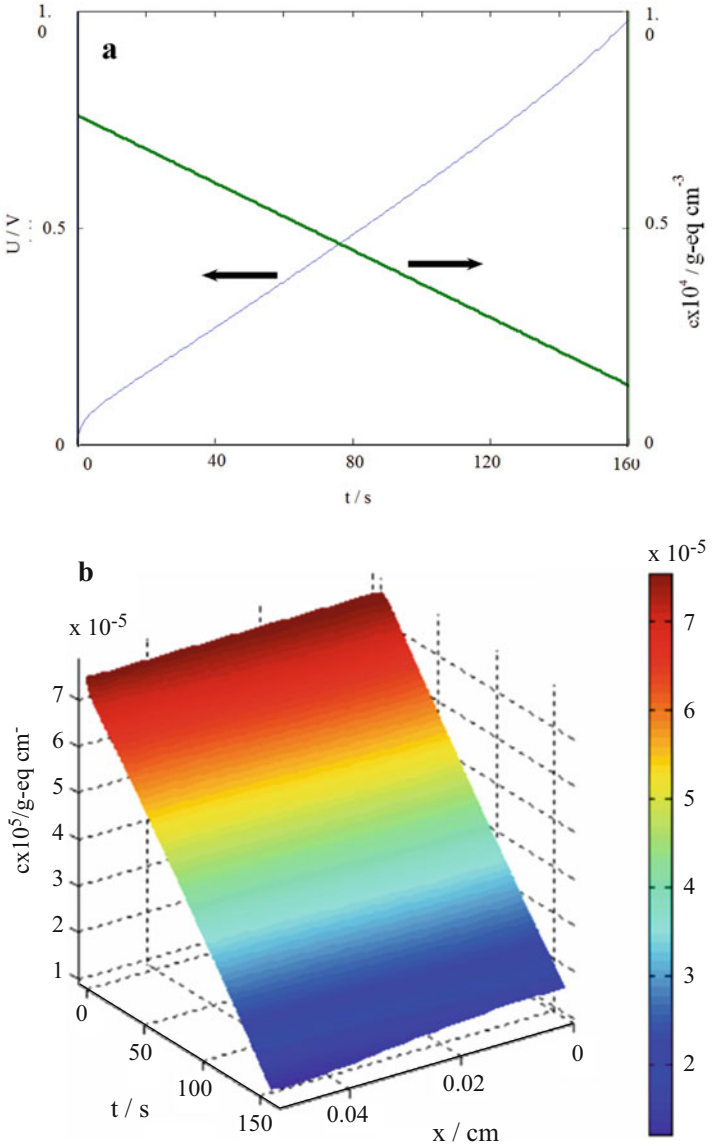

Fig. 9.8 Numerical solution of the voltage and mean concentration in the cell (**a**) and time evolution of the profile concentration in the half-cell (**b**). The CH900 electrode was used; the initial concentration of the $NaHCO_3$ solution was 0.075 mg-eq cm^{-3}

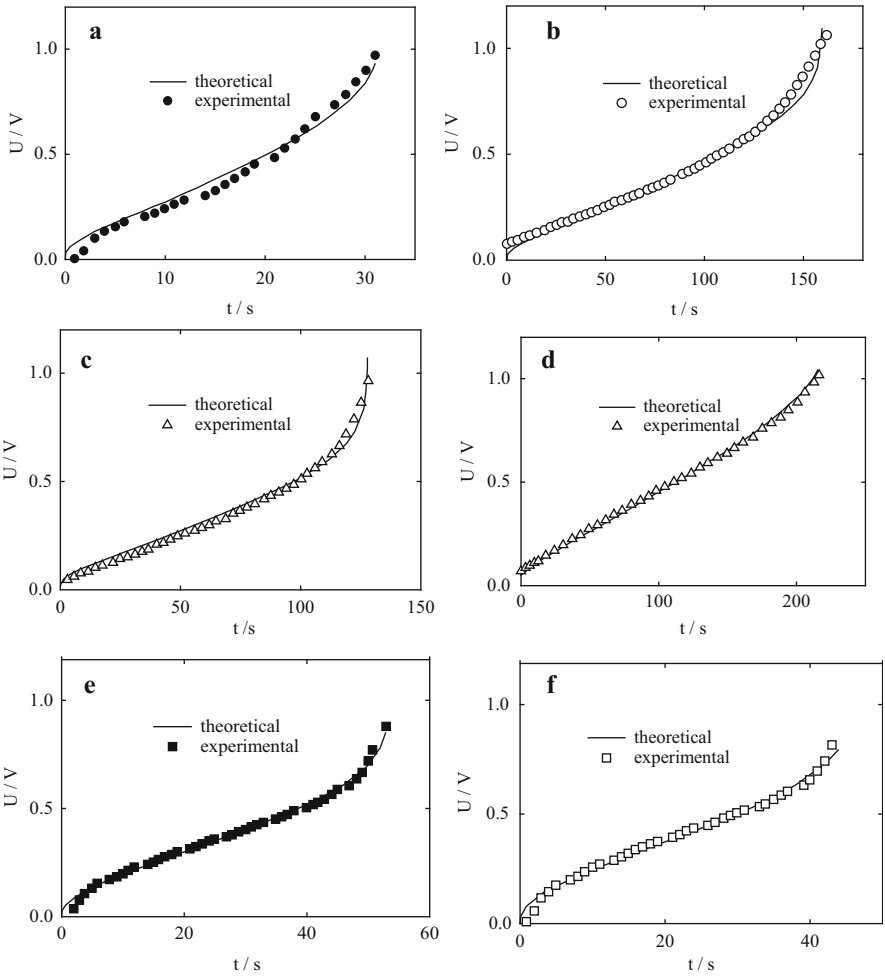

Fig. 9.9 Experimental and theoretical galvanostatic charging curves for the CH900 (**a**) VISKUMAK (**b**-**d**) and SAIT (**e**, **f**) electrodes. A solution contained a mixture of $CaCl_2$. $NaHCO_3$ and $MgSO_4$ concentration of each salt was 0.0257 M (a); 0.1 N single-component solutions were also used: $NaHCO_3$ (**b**, **e**), $CaCl_2$ (**c**), and $MgSO_4$ (**d**, **f**). $I = 2.8$ (**a**–**e**) and 10 (**f**) mA cm^{-2}

theoretical and experimental curves agree well with each other, which points to correctness of the model. In some cases, total experimental electrochemical adsorption capacity was slightly lower as compared with the theoretical values. This is probably due to adsorption of a certain amount of species on highly developed surface of carbon electrodes before polarization during measurements of discharge curves. Similar specific adsorption was observed earlier [46].

The charging-discharging curves simulate deionization-concentrating inside the static cell containing the CH900 electrodes (Fig. 9.10). The curves are plotted in the

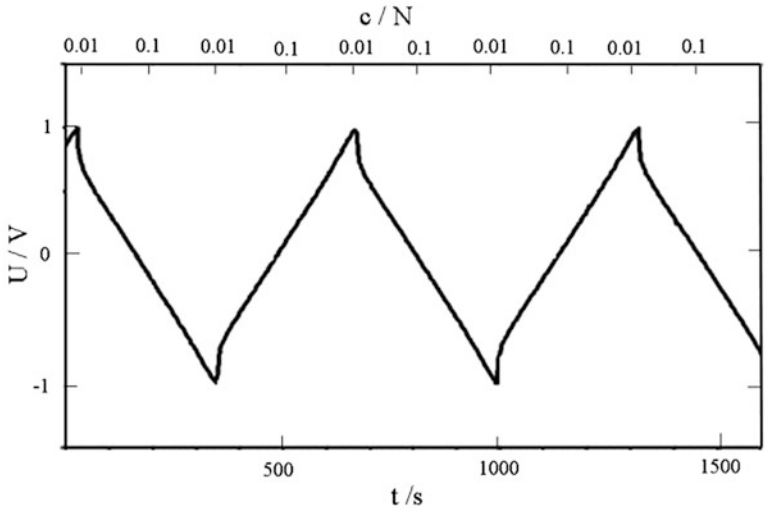

Fig. 9.10 Cyclic galvanostatic curves for the cell containing CH900 electrodes. The 0.1 N $CaCl_2$ solution was used, I=10 mA cm^{-2}

coordinates of voltage-time-concentration of the solution inside the cell. Charging is accompanied by deionization, and concentrating occurs in the course of discharge. Each semi-cycle (i.e., stages of deionization and concentrating) passes from the minimum to the maximum and further from the maximum to the minimum.

9.10 Conclusions

Among investigated AC electrodes, the CH900 sample is the most optimal material for CDI processes. This electrode is characterized by the highest value of specific surface area caused by the largest total volume of micropores and nanosized voids. Moreover, the largest total and hydrophilic porosity is attributed to the CH900 electrode. At last, the largest volume of macropores, which provide high hydrodynamical permittivity, has been found for this material. This property is very important for a dynamic cell, through which the solution passes [56]. The largest hydrophilic specific surface causes the highest values of adsorption capacity and surface conductivity [52]. This causes minimal energy consumptions for pure water production. The prospective way for optimization of AC electrodes is to develop the materials, which are characterized simultaneously by the highest nanoporosity and significant volume of macropores. Macropores are able to provide the shortest time of charging-discharging.

The simple model, which is based only on experimental data (SC and EDL capacitance), has been developed. The model allows one to avoid difficult

calculations of the EDL. These calculations are complicated by features of porous structure of AC materials particularly narrowings-widenings of pores and their tortuosity.

Further investigations of CDI processes are related to development of high conductive separators that would be permeable toward cations and anions. Possible materials are polymer mosaic membranes [58]. Ceramic [59–61] or polymer membranes [62, 63] modified by nanoparticles of amphoteric inorganic ion exchanger could be considered as an alternative.

References

1. Nath K (2017) Membrane separation processes, 2nd edn. PHI Learning Private Limited, Delhi
2. Alvarado L, Chen A (2014) Electrodeionization: principles, strategies and applications. Electrochim Acta 132:583–597
3. Dzyazko YS, Ponomareva LN, Volfkovich YM et al (2013) Conducting properties of a gel ionite modified with zirconium hydrophosphate nanoparticles. Russ J Electrochem 49 (3):209–215
4. Dzyaz'ko YS, Rozhdestvenskaya LM, Pal'chik AV (2005) Recovery of nickel ions from dilute solutions by electrodialysis combined with ion exchange. Russ J Appl Chem 75:414–421
5. Dzyazko YS, Volfkovich YM, Ponomaryova LN et al (2016) Composite ion-exchangers based on flexible resin containing zirconium hydrophosphate for electromembrane separation. J Nanosci Technol 2(1):43–49
6. Oren Y (2008) Capacitive deionization (CDI) for desalination and water treatment—past, present and future (a review). Desalination 228:10–29
7. Avraham E, Noked M, Bouhadana Y et al (2009) Limitations of charge efficiency in capacitive deionization II. On the behavior of cdi cells comprising two activated carbon electrodes. J Electrochem Soc 156(10):157–162
8. Suss ME, Baumann TF, Bourcier WL et al (2012) Capacitive desalination with flow-through electrodes. Energy Environ Sci 5:9511–9519
9. Rica RA, Ziano R, Salerno D et al (2012) Thermodynamic relation between voltage-concentration dependence and salt adsorption in electrochemical cells. Phys Rev Lett 109:156103. https://doi.org/10.1103/PhysRevLett.109.156103
10. Porada S, Zhao R, van der Wal A et al (2013) Review on the science and technology of water desalination by capacitive deionization. Prog Mater Sci 58(8):1388–1442
11. Jande YAC, Kim WS (2013) Desalination using capacitive deionization at constant current. Desalination 329:29–34
12. Soffer A, Folman M (1972) The electrical double layer of high surface porous on carbon electrode. Electroanal Chem 38(1):25–43
13. Jande YAC, Kim WS (2013) Predicting the lowest effluent concentration in capacitive deionization. Sep Purif Technol 115:224–230
14. Li H, Pan L, Lu T et al (2011) A comparative study on electrosorptive behavior of carbon nanotubes and graphene for capacitive deionization. J Electroanal Chem 653(1–2):40–44
15. Gabelich CJ, Tran TD, Suffet IH (2002) Electrosorption of inorganic salts from aqueous solution using carbon aerogels. Environ Sci Technol 36(13):3010–3019
16. Li H, Lu T, Pan L et al (2009) Electrosorption behavior of graphene in NaCl solutions. J Mater Chem 19:6773–6779
17. Wang G, Dong Q, Ling Z (2012) Hierarchical activated carbon nanofiber webs with tuned structure fabricated by electrospinning for capacitive deionization. J Mater Chem 22:21819–21823

18. Gaikwad MS, Balomajumder C (2016) Polymer coated capacitive deionization electrode for desalination: a mini review. Electrochem Energy Technol 2(1). https://doi.org/10.1515/eetech-2016-0001
19. Liu Y, Nie C, Liu X et al (2015) Review on carbon-based composite materials for capacitive deionization. RSC Adv 5:15205–15225
20. Zhang D, Wen X, Shi L et al (2012) Enhanced capacitive deionization of graphene/mesoporous carbon composites. Nanoscale 4:5440–5446
21. Myint MTZ, Dutta J (2012) Fabrication of zinc oxide nanorods modified activated carbon cloth electrode for desalination of brackish water using capacitive deionization approach. Desalination 305:24–30
22. Vol'fkovich YM, Sosenkin VE, Nikol'skaya NF et al (2008) Porous structure and hydrophilic-hydrophobic properties of gas diffusion layers of the electrodes in proton-exchange membrane fuel cells. Russ J Electrochem 44(3):278–285
23. Bagotzky VS, Kazarinov VE, Vol'fkovich YM et al (1989) Macrokinetic study of thionyl chloride reduction on porous carbon electrodes. J Power Sources 26(3–4):427–433
24. Volfkovich YM, Bagotzky VS (1994) The method of standard porosimetry 2. Investigation of the formation of porous structures. J Power Sources 48(3):339–348
25. Newman J, Thomas-Alyea KE (2004) Electrochemical systems, 3rd edn. Wiley, Hoboken
26. Newman J, Tiedemann W (1975) Porous electrode theory with battery applications. AICHE J 21:25–41
27. Conway BE (1999) Electrochemical supercapacitors: scientific fundamentals and technological applications. Kluwer Academic Publishers-Plenum Publishers, New York
28. De Levie R (1963) On porous electrodes in electrolyte solutions. I. Capacitance effects. Electrochim Acta 8(10):751–780
29. De Levie R (1964) On porous electrodes in electrolyte solutions—IV. Electrochim Acta 9 (9):1231–1245
30. Srinivasan V, Weidner JW (1999) Mathematical modeling of electrochemical capacitors. J Electrochem Soc 146:1650–1658
31. Volfkovich YM, Bograchev DA, Mikhalin AA et al (2013) Supercapacitor carbon electrodes with high capacitance. J Solid State Electrochem 18(5):1351–1363
32. Yang K-L, Ying T-Y, Yiacoumi S et al (2001) Electrosorption of ions from aqueous solutions by carbon aerogel: an electrical double-layer model. Langmuir 17(6):1961–1969
33. Ying T-Y, Yang K-L, Yiacoumi S et al (2002) Electrosorption of ions from aqueous solutions by nanostructured carbon aerogel. J Colloid Interface Sci 250(1):18–27
34. Johnson AM, Newman J (1971) Desalting by means of porous carbon electrodes. J Electrochem Soc 118(3):510–517
35. Vol'fkovich YM, Mazin VM, Urisson NA (1998) Operation of double-layer capacitors based on carbon materials. Russ J Electrochem 34(8):740–746
36. Verbrugge MW, Liu P (2005) Microstructural analysis and mathematical modeling of electric double-layer supercapacitors. J Electrochem Soc 152(5):D79–D87
37. Biesheuvel PM, Bazant MZ (2010) Nonlinear dynamics of capacitive charging and desalination by porous electrodes. Phys Rev E 81(3):031502
38. Biesheuvel PM, Fu Y, Bazant MZ (2012) Electrochemistry and capacitive charging of porous electrodes in asymmetric multicomponent electrolytes. Russ J Electrochem 48(6):580–592
39. Mani A, Bazant MZ (2011) Deionization shocks in microstructures. Phys Rev E 84(6):061504. https://doi.org/10.1103/PhysRevE.84.061504
40. Biesheuvel PM, Porada S, Levi M, Bazant MZ (2014) Attractive forces in microporous carbon electrodes for capacitive deionization. J Solid State Electrochem 18(5):1365–1376
41. Volfkovich YM, Sosenkin VE (2012) Porous structure and wetting of fuel cell components as the factors determining their electrochemical characteristics. Russ Chem Rev 86(6):936–959
42. Volfkovich YM, Bagotsky VS, Filippov AN (eds) (2014) Porous materials and powders used in different fields of science and technology. Springer-Verlag, London/Heidelberg/New York/Dordrecht

43. Volfkovich YM, Sakars AV, Volinsky AA (2005) Application of the standard contact porosimetry for nanomaterials. Int J Nanotechnol 2(3):292–302
44. Rouquerol J, Baron G, Denoyel R et al (2012) Liquid intrusion and alternative methods for the characterization of macroporous materials (IUPAC technical report). Pure Appl Chem 84 (1):107–136
45. Vol'fkovich YM, Sosenkin VE, Nikol'skaya NF (2010) Hydrophilic-hydrophobic and sorption properties of the catalyst layers of electrodes in a proton-exchange membrane fuel cell: a stage-by-stage study. Russ J Electrochem 46(4):438–449
46. Gladysheva TD, Shkol'nikov EL, Vol'fkovich YM et al (1982) The porous structure of dispersed platinum. Elektrokhimiya 18(4):435–442
47. Kononenko N, Nikonenko V, Grande D et al (2017) Porous structure of ion exchange membranes investigated by various techniques. Adv Colloid Interface Sci 246:196–216
48. Dzyazko YS, Perlova OV, Perlova NA et al (2017) Composite cation-exchange resins containing zirconium hydrophosphate for purification of water from U(VI) cations. Desalin Water Treat 69:142–152
49. Jeffery JH, Bassett J, Menoham J et al (1989) Vogel's textbook on quantitative chemical analysis, 5th edn. Longman Scientific and Technical – Wiley, Harlow/New York
50. Berezina NP, Kononenko NA, Dyomina OA et al (2008) Characterization of ion-exchange membrane materials: properties vs structure. Adv Colloid Interf Sci 139(1–2):3–28
51. Dzyazko Y, Rozhdestvenska L, Palchik A, Lapicque F (2005) Ion-exchange properties and mobility of Cu^{2+} ions in zirconium hydrophosphate ion exchangers. Sep Purif Technol 45 (2):141–146
52. Vol'fkovich YM, Mikhalin AA, Rychagov AY (2013) Surface conductivity measurements for porous carbon electrodes. Russ J Electrochem 49(6):594–598
53. Galama AH, Post JW, Cohen Stuart MA et al (2013) Validity of the Boltzmann equation to describe Donnan equilibrium at the membrane-solution interface. J Memb Sci 442:131–139
54. Andersen MB, Van Soestbergen M, Mani A et al (2012) Current-induced membrane discharge. Phys Rev Lett 109(10):108301. https://doi.org/10.1103/PhysRevLett.109.108301
55. Chizmadzhev Y, Markin V, Tarasevich M et al (1971) Macrokinetics of processes in porous media. Nauka, Moscow
56. Archie GE (1952) Classification of carbonate reservoir rocks and petrophysical considerations. Am Assoc Pet Geol Bull 36(2):278–298
57. Skeel RD, Berzins M (1990) A method for the spatial discretization of parabolic equations in one space variable. SIAM J Sci Stat Comput 11(1):1–32
58. Volfkovich YM, Rychagov AY, Mikhalin AA et al (2018) Capacitive deionization of water using mosaic membrane. Desalination 426:1–10
59. Dzyaz'ko YS, Belyakov VN, Vasilyuk SL et al (2006) Anion-exchange properties of composite ceramic membranes containing hydrated zirconium dioxide. Russ J Appl Chem 79(5):769–773
60. Dzyazko YS, Volfkovich YM, Sosenkin VE et al (2014) Composite inorganic membranes containing nanoparticles of hydrated zirconium dioxide for electrodialytic separation. Nanoscale Res Lett 9:271. https://doi.org/10.1186/1556-276X-9-271
61. Martı-Calatayud MC, Garcıa-Gabaldon M, Perez-Herranz V et al (2015) Ceramic anion-exchange membranes based on microporous supports infiltrated with hydrated zirconium dioxide. RSC Adv 5:46348–46358
62. Pang R, Li X, Li J et al (2014) Preparation and characterization of ZrO_2/PES hybrid ultrafiltration membrane with uniform ZrO_2 nanoparticles. Desalination 332:60–66
63. Myronchuk VG, Dzyazko YS, Zmievskii YG et al (2016) Organic-inorganic membranes for filtration of corn distillery. Acta Periodica Technologica 47:153–165